Energy Engineering

Tech Science Press

https://doi.org/10.32604/ee.2026.078123

ARTICLE

Dynamic Modeling and Transient Analysis of Micro Reactor with Direct Helium Brayton Cycle Based on Modelica

Yunlong Li[1,*], Yuer Zhao[1], Li Pan[2], Huimin Zhang[1] and Jun Wang[1]

[1]China Nuclear Power Engineering Co., Ltd., Beijing, China
[2]Suzhou Tongyuan Soft & Ctrl Technology Co., Ltd., Suzhou, China

*Corresponding Author: Yunlong Li. Email: duke350@163.com

Received: 24 December 2025; Accepted: 10 February 2026; Published: 18 October 2026

ABSTRACT: Micro Gas-Cooled Reactor (MGCR) has garnered attention in relevant domains, owing to its advantages of miniaturization and transportability, which is capable of providing stable electrical power to off-grid and special regions. As a typical multi-physics coupled system, a dynamic model for the MGCR integrating nuclear, thermal-hydraulic, mechanical, and electrical subsystems was developed in this study using the multi-physics modeling language Modelica. Steady-state validation results indicate that the maximum deviation between the simulated values and the design parameters is merely 1.05%. Meanwhile, transient validation demonstrates a high degree of consistency with the outcomes generated by the MGT-3D code, with the relative error of the maximum temperature remaining below 3%. Based on the established dynamic model, transient analyses were carried out for three typical accident scenarios: reactivity insertion accidents, loss-of-flow accidents, and load rejection events. The results demonstrate that in the case of reactivity insertion and loss-of-flow accidents, the reactor can achieve a new steady state or autonomously reduce power through its inherent feedback mechanisms, thereby ensuring operational safety; specifically, the maximum temperature rise at the reactor outlet reaches 33.89°C during a reactivity insertion accident and 23°C in the event of a loss-of-flow accident. For load rejection scenarios, the opening of the isolation valve can effectively protect the helium turbine: upon a complete loss of external load, the rotor speed increases by up to 5.6%, which does not exceed the safety limits. This study verifies the inherent safety of MGCRs under accident conditions and demonstrates the application potential of Modelica in multi-physics dynamic analyses of such advanced nuclear systems.

KEYWORDS: Micro gas-cooled reactor; dynamic modeling; transient analysis; Modelica

1 Introduction

In recent years, MGCR has emerged as a new direction in nuclear energy development. Due to their advantages, such as miniaturization, transportability, and stable energy supply capacity, MGCR exhibits broad application prospects in special scenarios, including remote areas, plateaus, islands, and post-disaster reconstruction [1,2]. Their modular design facilitates batch manufacturing, vehicular transport, and rapid on-site deployment, which not only shortens the construction period but also enhances economic viability [3,4]. Compared with traditional commercial pressurized water reactors, gas-cooled microreactors possess the advantages of a more compact system configuration and more streamlined operating procedures. Nevertheless, they are confronted with challenges in high-precision equipment manufacturing technologies and a lack of comprehensive understanding of their system-level operational characteristics. This knowledge gap hinders the development of safe operation strategies; furthermore, the engineering maturation of this technology requires in-depth research into system modeling and transient behavior analysis.

Copyright © 2026 The Authors. Published by Tech Science Press. This work is licensed under a Creative Commons Attribution 4.0 International License, which permits unrestricted use, distribution, and reproduction in any medium, provided the original work is properly cited.

The MGCR fuel assembly adopts a hexagonal graphite block structure, with coolant channels and fuel rods arranged in a triangular lattice within the assembly. The fuel rods consist of pellets with SiC as the matrix, in which TRISO fuel particles [5] are dispersed. Helium is employed as the coolant. This reactor type features high power density and inherent safety. The energy conversion system operates on a direct helium Brayton cycle, which mainly consists of a turbine, a regenerator, a precooler, a high-pressure compressor, an intercooler, a low-pressure compressor, and a permanent magnet synchronous generator. The turbine, high-pressure compressor, low-pressure compressor, and generator are coaxial. The helium heated by the reactor core expands through the turbine, converting thermal energy into mechanical work to drive the coaxial compressors and generator. The precooler and intercooler are installed upstream of the high-pressure and low-pressure compressors, respectively, to improve cycle efficiency. This design simplifies the reactor system and enhances compactness. Meanwhile, the system employs only a single circuit connecting the reactor core to the generator, together with coaxial rotating equipment, resulting in strong internal coupling effects. Therefore, dynamic modeling is indispensable for analyzing its transient behavior. Fig. 1 shows the system flowchart of the MGCR. Fig. 2 presents the Modelica model of the MGCR. Fig. 3 depicts the cross-section of the reactor core.

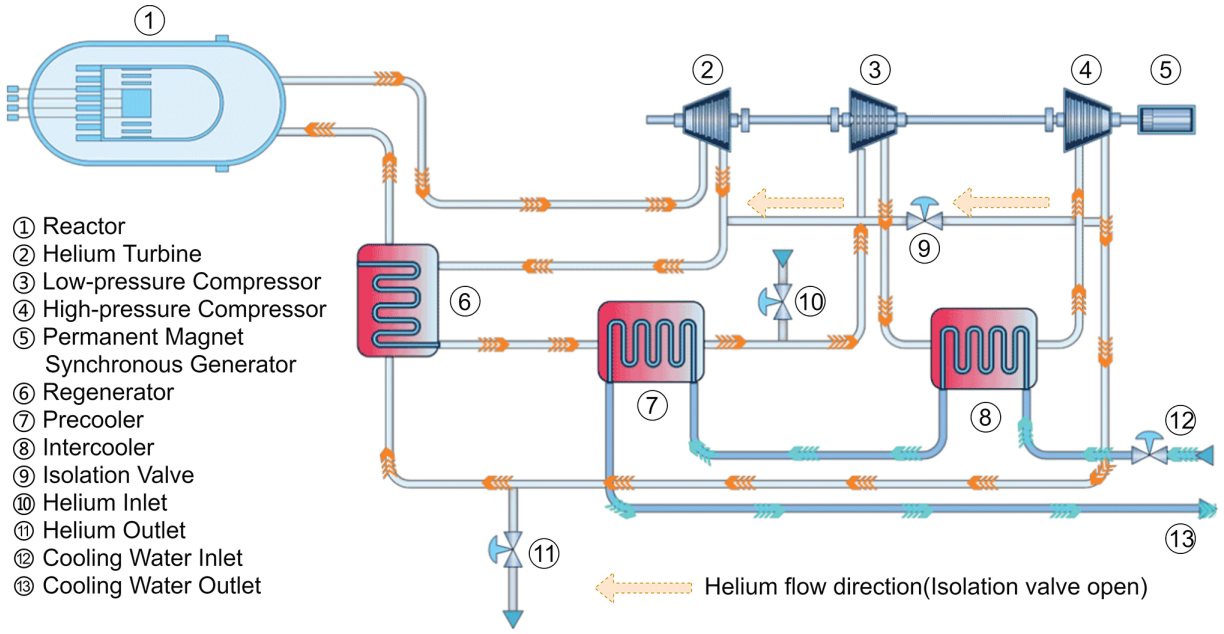


Figure 1: Flow diagram of the MGCR.

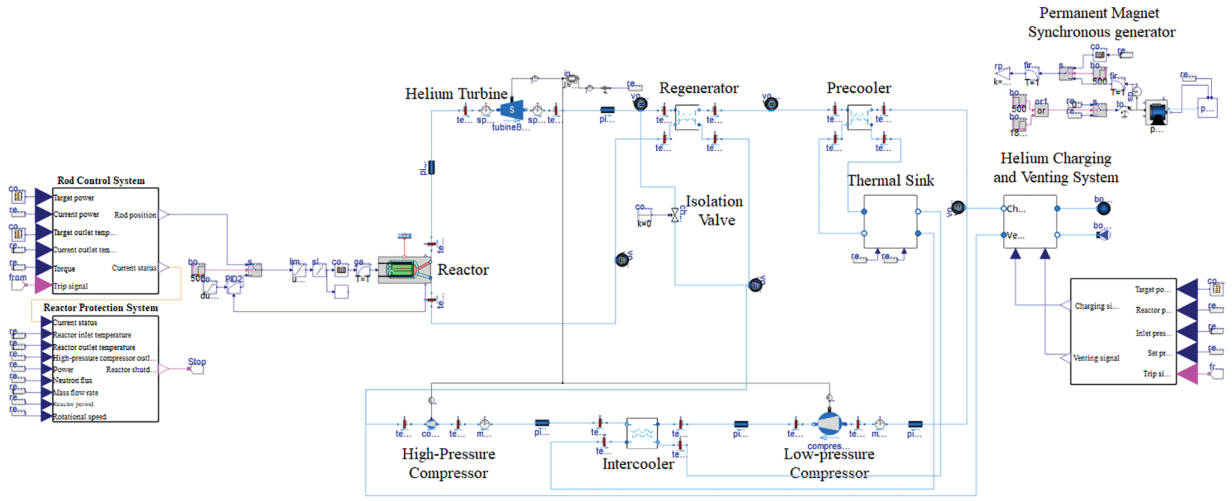


Figure 2: Modelica model layout of the MGCR.

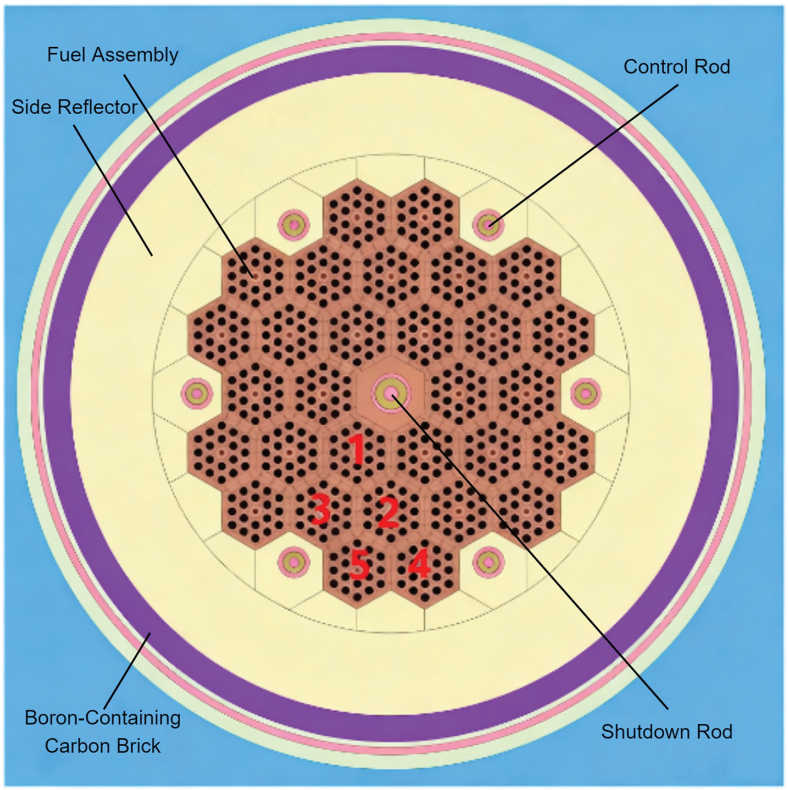


Figure 3: Cross-section of the reactor core.

To develop a dynamic reactor model with simplicity, efficiency, and modularity, appropriate modeling tools are essential. Modelica is an object-oriented, declarative, acausal modeling language with multi-domain physical systems modeling capabilities [6]. In Modelica, a system model is represented by a set of coupled differential-algebraic equations (DAE) and discrete equations, which can accurately depict the behavior of various physical processes.

The interactions between sub-models are represented by connection equations, which eliminate the need to specify any causal relationships. These models exhibit reproducibility. Additionally, Modelica has extensive third-party libraries covering materials, media, heat transfer, fluids, mechanics, and electricity, which significantly reduce the complexity of model development.

Numerous studies have focused on the application of Modelica in reactor system modeling and dynamic modeling. A Modelica-based model of the VVER-1200 reactor is established by Reference [7], which accurately describes reactor dynamic behavior. A complete transient thermal-hydraulic analysis model was developed for an SCO_2 Brayton cycle reactor using Modelica by Reference [8], enabling precise simulation of the reactor's transient operating conditions through the coupled simulation of core physics and thermal-hydraulics. The modeling method and control system of the Helium Brayton cycle high-temperature gas-cooled reactor were studied by Reference [9], and an operational control scheme was proposed. The results show that the control system effectively realizes load-following operation under a 33% external load variation. A system analysis program for an SCO_2 Brayton cycle reactor was developed by Reference [10], and the transient characteristics analysis reveals that the system exhibits a rapid load change response and maintains safe operation across various power levels. A tritium breeding system analysis tool was developed by Reference [11], with results showing good agreement with analytical solutions. The Modelica model also possesses excellent simulation capabilities for the SCO_2 reactor of the EU-DEMO project by Reference [12]. A dynamic model of a space He-Xe Brayton cycle reactor is established by Reference [13]. The results of accident condition analysis show that minor cold-end accidents allow autonomous power adjustment via system stability. Specifically, a 30% reduction in NaK coolant flow led to a 2.22% decrease in power generation efficiency and a 5.79% drop in cycle efficiency.

Nevertheless, current studies predominantly focus on traditional pressurized water reactors and SCO_2-cooled reactors, with limited research dedicated to helium direct cycle reactors. Many analyses only address single or a few physical fields, lacking integrated multi-physics analyses (nuclear, thermal, mechanical, electrical), and transient accident analyses for helium direct cycle reactors are scarce. Moreover, applications of Modelica in this specific field are relatively underdeveloped. In this study, mechanistic models were developed for reactor components, with the turbine and compressor models validated against experimental data. Subsequently, an integrated dynamic model was constructed and verified by comparing its results with the design steady-state parameters and transient simulation outcomes from other programs. Finally, transient response analyses were conducted for various accident conditions of the reactor, providing valuable insights for the design of the helium direct cycle reactor.

2 Models and Methods

A dynamic model for the MGCR was developed using Modelica, which can predict the dynamic performance under various operating conditions. Modelica's robust standard and third-party libraries were utilized where possible. The mathematical models of key components are described below.

2.1 Nuclear Reactor System

The nuclear reactor system mainly includes the point kinetics model and the reactor thermal-hydraulic model. The point kinetics model is employed to calculate the total core power output, with the assumption that the heat source is directly generated in the fuel assembly and subsequently transferred to the helium flowing through the coolant channels. The interference effects of CRs (Control Rods) are neglected.

2.1.1 Point Kinetics Model

The total reactivity is determined by four distinct components: initial reactivity, ^{135}Xe reactivity, temperature reactivity, and control rod reactivity.

Assuming a spatially uniform neutron flux distribution and constant temperature feedback coefficients, the point kinetics equations are given in Eqs. (1)–(3) [14]. The key parameters used in the point kinetics model are shown in Table 1, which were calculated using the RMC code [15].

Table 1: Key parameter of the point kinetics model.

Parameter	Value	Parameter	Value
$\sum_f$	3.61E−03 cm^{-1}	υ	2.44
γ_I	0.0635	γ_{Xe}	0.00432
Λ	0.00134 s	α_T	−2.62
β_1	2.47E−04	λ_1	0.0127
β_2	1.385E−03	λ_2	0.0317
β_3	1.222E−03	λ_3	0.116
β_4	2.645E−03	λ_4	0.311
β_5	8.32E−04	λ_5	1.397
β_6	1.69E−04	λ_6	3.876

$$\frac{dn(t)}{dt} = \frac{\rho - \beta}{\Lambda} n(t) + \sum_{i=1}^{6} \lambda_i C_i(t), \tag{1}$$

$$\frac{dC_i(t)}{dt} = \frac{\beta_i}{\Lambda} n(t) - \lambda_i C_i(t), \tag{2}$$

$$\beta = \sum_{i=1}^{6} \beta_i, i = 1, 2, \ldots, 6. \tag{3}$$

In thermal neutron reactors, ^{135}Xe is an important isotope due to its large thermal neutron absorption cross-section. ^{135}Xe is primarily produced through two pathways: one is direct generation from fission, and the other is via the decay of ^{135}I. These relationships are shown in Eqs. (4)–(6).

$$\frac{dn_I(t)}{dt} = \gamma_I \sum_f \phi - \lambda_I n_I(t), \tag{4}$$

$$\frac{dn_{Xe}(t)}{dt} = \gamma_{Xe} \Sigma_f \phi + \left(\lambda_{Xe} + \sigma_a^{Xe} \phi\right) n_{Xe}(t) \tag{5}$$

$$\rho_{Xe} = \frac{-10^{-24} \sigma_a^{Xe} n_{Xe} c_t}{\upsilon \Sigma_f}. \tag{6}$$

The temperature reactivity feedback is considered as a collective effect arising from the temperature variations of the fuel, coolant, matrix material, and reflector components. The temperature-dependent reactivity is quantified by Eq. (7).

$$\rho_T = \alpha_T \left(T_{ave} - T_{ref} \right). \tag{7}$$

Control rod reactivity is induced by control rod movement, without considering interference effects or spatial power distribution changes. The control rod integral worth is shown in Fig. 4, which is derived from RMC calculations [15].

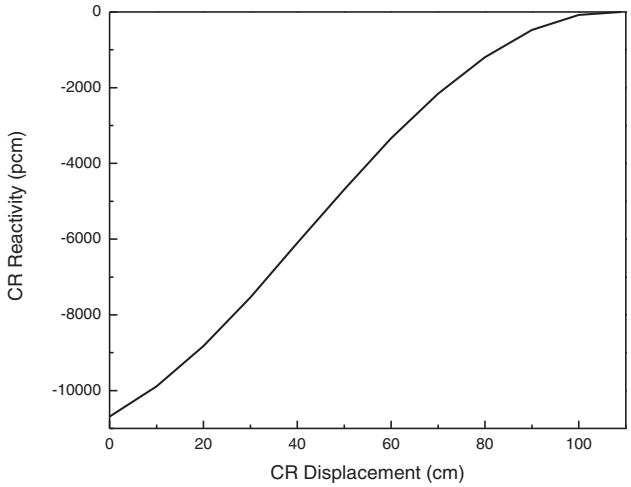


Figure 4: CR integral worth curve.

The comprehensive formula for calculating the total core reactivity is presented in Eq. (8).

$$\rho = \rho_{ini} + \rho_{Xe} + \rho_T + \rho_{CR}. \tag{8}$$

2.1.2 Reactor Thermal-Hydraulic Model

To construct the reactor thermal-hydraulic model [16–18], the standard Modelica libraries were utilized to provide components for heat transfer and material property calculations. Specifically, helium properties were obtained from IdealGases.SingleGases. He, while components like pipes and thermal resistance were sourced from the Thermal and Fluid libraries. In this study, helium is regarded as an ideal gas, and the helium transport pipelines are simplified as smooth-walled in the thermodynamic model.

The basic heat balance is given in Eqs. (9)–(12).

$$M_j C_j \frac{dT_j}{dt} = Q_{f,j} + Q_{o,j} - Q_{s,j}, \tag{9}$$

$$Q_{f,j} = \sum_f \phi Q_1, \tag{10}$$

$$Q_{s,j} = h_{He,j} A_{s,j} \left(T_{b,j} - T_{He,j} \right) / d_j, \tag{11}$$

$$Q_{o,j} = Q_{o,j-1} + Q_{o,j+1}. \tag{12}$$

Helium convection heat transfer in the tube considers turbulent, laminar, and transition flows. The convective heat transfer coefficient is calculated by Eqs. (13)–(17).

$$h_{He} = \frac{\chi_{He}}{D}\mathrm{Nu}_{He}, \tag{13}$$

$$Nu_{He} = \begin{cases} 2\left(\frac{m_{He}C_{p,He}}{\chi_{He}l}\right)^{0.333} & Re < 2000 \\ 0.023Re^{0.8}Pr^{0.4} & Re \geq 2000 \end{cases}, \tag{14}$$

$$Re_{He} = \frac{\rho_{He}v_{He}D}{\mu_{He}}, \tag{15}$$

$$Pr_{He} = \frac{C_{p,He}\mu_{He}}{\chi_{He}}, \tag{16}$$

$$v_{He} = \frac{v_{m,He}}{\rho_{He}A_{He}}. \tag{17}$$

The flow regime classification method employed in the LocalPipeFlowHeatTransfer model follows the criteria: for Re > 10,000, it is turbulent flow; for Re < 2300, it is laminar flow; and for Re between 2300–10,000, Nu is calculated via Modelica's spline Function.

Flow pressure drop is determined by the flow resistance. The pressure drop in the coolant channel is given by Eqs. (18) and (19).

$$dp_{He,j} = \kappa_{He,j}\frac{l_{He,j}}{D_{\mathrm{He},j}}\frac{\rho_{He,j}v_{He,j}^2}{2}, \tag{18}$$

$$\kappa_{He,j} = \begin{cases} \frac{64}{Re_{He,j}} & Re_{He,i} < 1600 \\ 0.11\left(\frac{68}{Re_{He,j}}\right)^{0.25} & Re_{He,i} \geq 1600 \end{cases}. \tag{19}$$

2.2 Energy Conversion System Model

The energy conversion system includes the turbine, the regenerator, the high-pressure compressor, the low-pressure compressor, the permanent magnet synchronous generator, the precooler, the intercooler, and the isolation valve.

2.2.1 Turbine

The turbine converts the thermal energy of the fluid into mechanical energy. The helium heated by the reactor core expands through the turbine's blades, driving the impeller to rotate and thereby generating mechanical work. The flow equations are given by Eqs. (20) and (21), and the energy equations are given by Eqs. (22) and (23) [19].

The mechanistic model is compared with experimental measurements in Fig. 5, showing errors within 10%. The measured data are derived from the experimental results of the turbine custom-designed and manufactured for the MGCR, for which a dedicated test rig was built to acquire the experimental data. The vertical axis of corrected flow represents $m_{He}\sqrt{T_{in}}/P_{in}$.

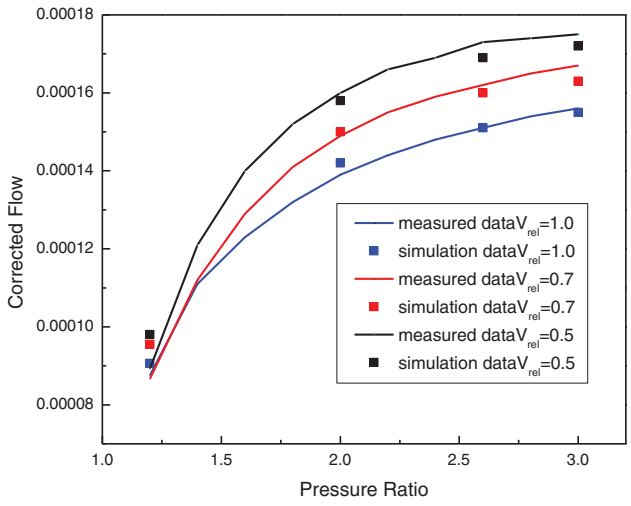


Figure 5: Mechanistic model verification diagram of the turbine.

$$m_{He} = K_t \sqrt{p_{in}\rho_{in}\left(1-\left(\frac{p_{out}}{p_{in}}\right)^2\right)}, \tag{20}$$

$$K_t = \frac{m_{He,nor}}{\sqrt{p_{in,nor}\rho_{in,nor}\left(1-\left(\frac{p_{out,nor}}{p_{in,nor}}\right)^2\right)}}, \tag{21}$$

$$\Delta h \cdot \eta_h \cdot m_{He} \cdot \eta_m = -\tau \cdot v_r, \tag{22}$$

$$\eta_h = \eta_{h,nor} - \partial_t \left(\frac{v_r}{v_{r,nor}}\sqrt{\frac{h_{in,nor}-h_{out,nor}}{h_{in}-h_{out}}}-1\right)^2. \tag{23}$$

2.2.2 Compressor

The compressor is used to increase the pressure and temperature of the helium by consuming mechanical energy, thereby providing the kinetic energy required for the helium cycle. In this study, the same computational model is adopted for both the high-pressure compressor and the low-pressure compressor, which is based on the similarity principles of turbomachinery. The mass conservation equation is given by Eq. (24). The pressure equations are given by Eqs. (25)–(27) [20]. The energy conservation equation is given by Eq. (28). The mechanistic model is compared with measurements in Fig. 6, showing errors within 10%. The measured data are derived from the experimental results of the compressor custom-designed and manufactured for the MGCR, for which a dedicated test rig was built to acquire the experimental data. The vertical axis of corrected flow represents $m_{He}\sqrt{T_{in}}/P_{in}$.

$$\Delta m_{He} = m_{He,in} - m_{He,out}, \tag{24}$$

$$V_{He,\max} = V_{He,\max} v_r / v_{r,nor}, \tag{25}$$

$$\Delta p_{s,\max} = \Delta p_{\max} \left(v_r / v_{r,nor}\right)^2, \tag{26}$$

$$V_{He} = \frac{\Delta p_{s,\max} - \Delta p}{\Delta p_{\max}} \left(V_{He,\max} - V_{He,\min} \right) + V_{He,\min}, \tag{27}$$

$$\eta_h \cdot \Delta h = \frac{\kappa}{\kappa - 1} \frac{p_{in}}{p_{out}} \left(\frac{p_{out}}{p_{in}} \right)^{\left(\frac{\kappa-1}{\kappa} - 1 \right)}. \tag{28}$$

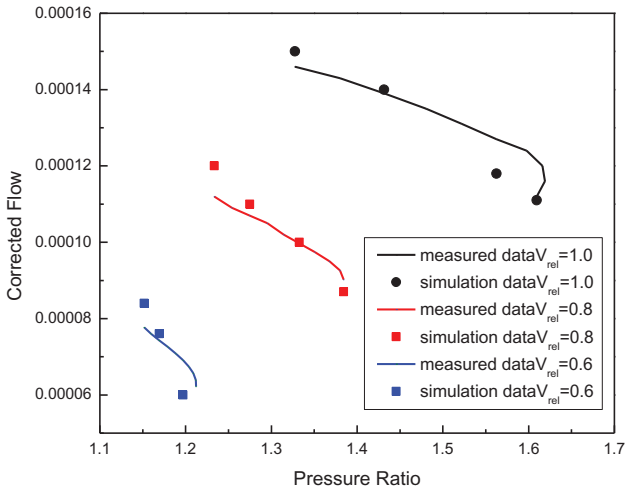


Figure 6: Mechanistic model verification diagram of the compressor.

2.2.3 Heat Exchanger

The main components of the heat exchanger model employed are the regenerator, the precooler, and the intercooler. A PCHE (Printed Circuit Heat Exchanger) is adopted for the regenerator, while both the precooler and the intercooler are of the PHE (plate heat exchanger) type. The heat capacity of the heat exchangers is neglected. The heat losses on the hot side and cold side of the heat exchangers are calculated by Eqs. (29) and (30). The heat exchanger efficiency is calculated by Eqs. (31) and (32). The pressure losses at both ends of the heat exchangers are calculated by Eq. (33). The flow velocity in the heat exchangers is calculated by Eq. (34) [16,17].

$$q_h = m_h c_p \left(h_{in,h} - h_{out,h} \right), \tag{29}$$

$$q_c = m_c c_p \left(h_{in,c} - h_{out,c} \right), \tag{30}$$

$$\eta_e = \frac{q_a}{q_{\max}}, \tag{31}$$

$$q_{\max} = C_{\min} \left(t_{in,h} - t_{in,c} \right), \tag{32}$$

$$\Delta p = 0.5 \cdot \varepsilon \cdot v_{flow}^2 \cdot \rho, \tag{33}$$

$$v_{flow} = \frac{m_{He}}{a_e \rho}. \tag{34}$$

2.2.4 Isolation Valve

The isolation valve is located on the bypass branch that is parallel to the mainline of the reactor core and the turbine. Its primary function is to mitigate the rotor overspeed during accidental conditions by diverting

a portion of the helium flow, thereby safeguarding the turbine from damage. The basic equations are given in Eqs. (35) and (36) [18].

$$m_{He} = A \cdot C_q \sqrt{\frac{2\Delta p}{\rho}} \tag{35}$$

$$A = \mu \cdot A_{\max} \tag{36}$$

2.2.5 Permanent Magnet Synchronous Generator

The permanent magnet synchronous generator is the main device for generating electrical energy, primarily realized through its mathematical model, which includes the voltage equation given by Eq. (37), stator flux equation given by Eq. (38), electromagnetic torque equation given by Eq. (39), and mechanical motion equation given by Eq. (40) [21,22].

$$\begin{cases} u_d = p_e \psi_d - \psi_q \omega + R_s i_d \\ u_q = p_e \psi_q - \psi_d \omega + R_s i_q \end{cases} \tag{37}$$

$$\begin{cases} \psi_d = L_d i_d + \psi_r \\ \psi_q = L_q i_q \end{cases} \tag{38}$$

$$T_e = p_e \left(i_q \psi_d - i_d \psi_q \right) \tag{39}$$

$$\frac{J}{p_e} \cdot \frac{d\omega}{dt} = T_e - T_L \tag{40}$$

3 Verification

Steady-state verification was conducted by comparing the steady-state calculation results with the design values. Meanwhile, transient verification was conducted by comparing the transient calculation results of the Anticipated Transients Without Scram (ATWS) with those generated by the MGT-3D code [23–25]. The ATWS accident is a severe incident which is selected as the representative transient scenario, since it encompasses a broad range of reactor operational conditions.

3.1 Steady-State Verification

The model established in Section 2 was verified by comparing its operating parameters with design values in steady-state operation conditions. The main parameters and relative errors are listed in Table 2. The results indicate that the maximum relative error across all parameters is merely 1.05%, which occurs at the outlet temperature of the low-pressure compressor. This minimal deviation demonstrates that the model can accurately replicate the steady-state behavior of the MGCR.

Table 2: Comparison of the MGCR design values and simulation values.

	Design Value	Simulation Value	Relative Error
Reactor			
Power (MW)	4.6	4.59	0.22%
Outlet temperature (°C)	749.61	747.53	0.28%
Outlet pressure (bar)	13.46	13.56	0.74%
Turbine			
Outlet temperature (°C)	507.52	506.03	0.29%

(Continued)

Table 2 (continued)

	Design Value	Simulation Value	Relative Error
Outlet pressure (bar)	5.85	5.86	0.17%
Regenerator hot side			
Outlet temperature (°C)	140.86	141.68	0.58%
Outlet pressure (bar)	5.73	5.72	0.17%
Precooler hot side			
Outlet temperature (°C)	34.85	34.69	0.46%
Outlet pressure (bar)	5.72	5.72	0.00%
Low-pressure compressor			
Outlet temperature (°C)	108.79	109.93	1.05%
Outlet pressure (bar)	9.02	9.01	0.11%
Intercooler hot side			
Outlet temperature (°C)	34.85	34.6	0.72%
Outlet pressure (bar)	8.78	8.79	0.11%
High-pressure compressor			
Outlet temperature (°C)	105.92	105.67	0.24%
Outlet pressure (bar)	13.62	13.68	0.44%

3.2 Transient Verification

The turbine and compressor models were verified during the modeling process. Transient verification was performed using the ATWS test data of the MGCR to validate the rationality of the reactor model. The ATWS test includes the rise in the reactor outlet temperature, which is the primary concern. When the simulation results are compared with those from MGT-3D, as shown in Fig. 7, the comparison reveals that the temperature evolution trends predicted by the two models are in excellent agreement. After the system stabilizes following the transient event, the relative errors between the average and maximum fuel temperatures predicted by the two models are within 3%.

4 Transient Analysis

To analyze transient characteristics of the MGCR, the established Modelica model was used to conduct calculations for accident conditions [26–28].

Based on typical accidents for similar reactors, reactivity insertion accidents and loss-of-flow accidents were analyzed for analysis. Meanwhile, the load rejection condition was also analyzed to study the rotor overspeed phenomenon.

4.1 Reactivity Insertion Accident

A reactivity insertion accident is typically triggered by the accidental ejection of a control rod during reactor operation, which introduces positive reactivity into the core and consequently leads to an increase in reactor power and coolant temperature.

Assumption: After the reactor has been operating stably at the rated condition for 500 s, one control rod is ejected instantly, introducing residual reactivity. The control rod position at steady state is 83 cm.

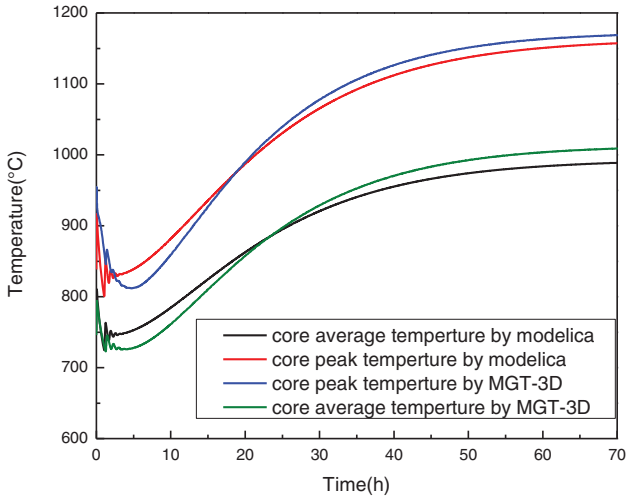
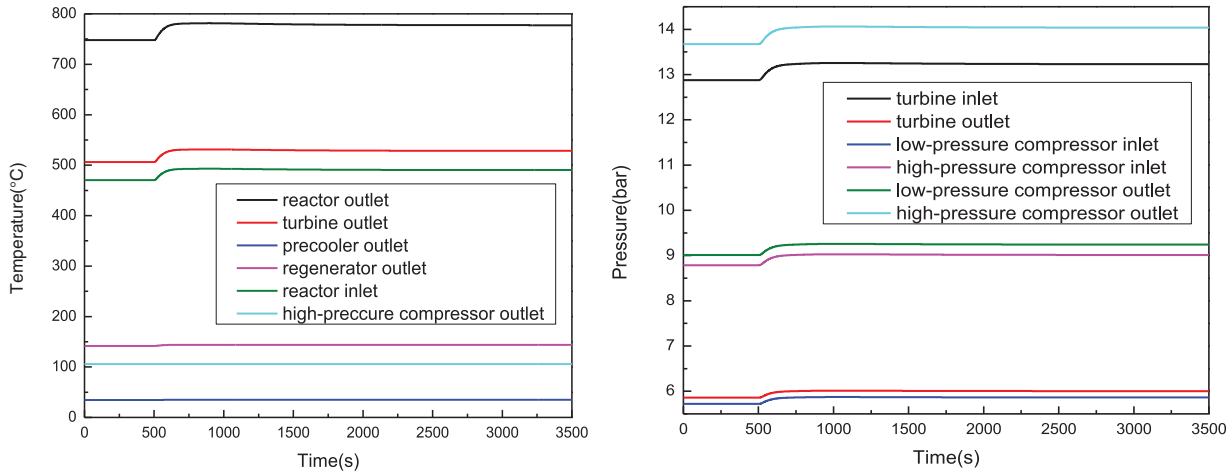


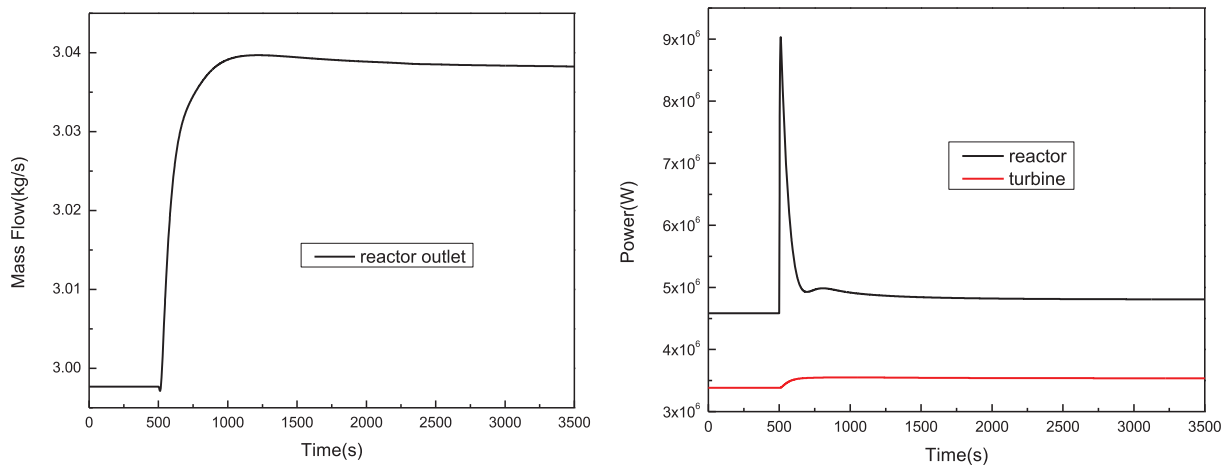
Figure 7: Transient verification diagram.

As shown in Fig. 8a–d, reactor power rapidly increases to a peak of about 9 MW, which induces a corresponding increase in the temperature. Due to the negative temperature feedback effect, the temperature rise introduces negative reactivity, which in turn reduces the reactor power.



(**a**) Temperature (**b**) Pressure

Figure 8: (Continued)



(**c**) Reactor outlet mass flow rate (**d**) Power

Figure 8: Main parameters variation diagram for reactivity insertion accident: (**a**) Temperature; (**b**) Pressure; (**c**) Reactor outlet mass flow rate; (**d**) Power.

The reactor outlet temperature rise increases the turbine outlet temperature. Owing to the effect of the regenerator, the reactor inlet temperature increases. The outlet temperature of the precooler remains stable due to its sufficient heat exchange capacity. Eventually, the reactor reaches a new steady state, exhibiting a 33.89°C increase in outlet temperature, a 0.36 bar increase in inlet pressure, a 0.04 kg/s mass flow increase, and a 0.22 MW power increase.

4.2 Loss-of-Flow Accident

During operation, the compressor may experience shaft jamming or breakage due to mechanical equipment failures, resulting in the loss of the driving source for helium. Alternatively, pipeline ruptures in the helium circulation loop due to component aging or external impact can also lead to a reduction in helium flow rate, thereby impairing the core's heat removal capacity.

Assumption: After the reactor has been operating stably at the rated condition for 500 s, a rupture accident occurs at the high-pressure compressor outlet, resulting in a rapid decrease in helium flow rate. Flow loss is shown in Fig. 9d.

As shown in Fig. 9a–c, when a rupture accident occurs, the flow rate in the loop decreases rapidly, the heat transfer capacity of the reactor declines, and the reactor outlet temperature rises, with a maximum increase of 23°C relative to the rated steady-state temperature. Eventually, the reactor loop is maintained at atmospheric pressure. Similar to the reactivity insertion accident scenario, the outlet temperature of the precooler remains stable throughout the transient process, due to its sufficient heat exchange capability.

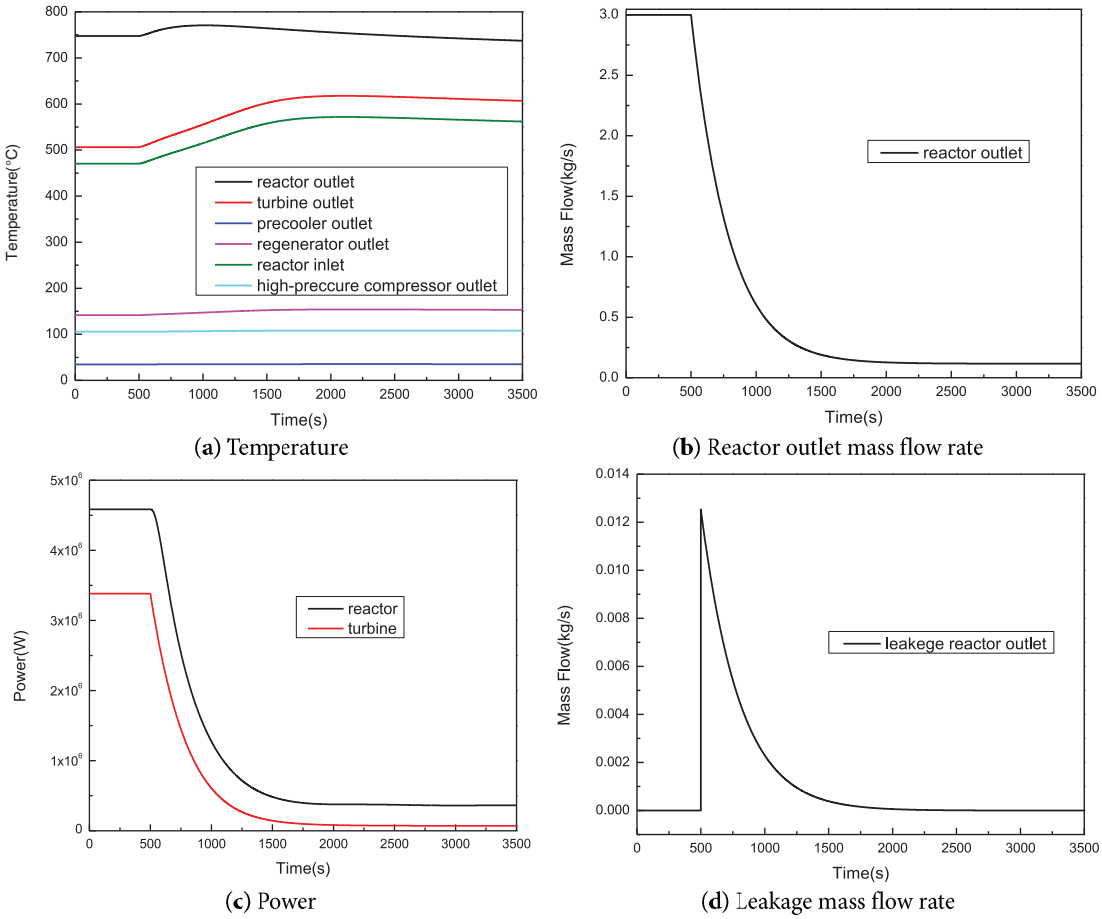


Figure 9: Main parameters variation diagram for loss-of-flow accident: (**a**) Temperature; (**b**) Reactor outlet mass flow rate; (**c**) Power; (**d**) Leakage mass flow rate.

4.3 Load Rejection Operating Condition

The turbine is the key component of the reactor. Excessive rotor speed can lead to structural failure of the turbine blades due to the enormous centrifugal forces, resulting in severe damage to the turbine. The main cause of turbine overspeed is the loss of turbine load.

Assumption: After the reactor has been operating stably at the rated condition for 500 s, the generator experiences a complete loss of external load, causing the rotor speed to increase of the coaxial rotating equipment. When the rotor speed exceeds the rated value by 1%, the isolation valve is triggered to open and instantly reaches 100% open position, allowing the helium at the outlet of the high-pressure compressor to bypass directly through the isolation valve branch.

As shown in Fig. 10a–d, the rotor speed increases, with a maximum rise of 5.6%. The increase in rotor speed enhances the helium circulation rate, which improves the core's heat removal capacity and leads to a slight decrease in the reactor outlet temperature. Concurrently, the reactor pressure increases by 0.77 bar. Thereafter, the isolation valve opens, causing the flow rate in the loop to decrease rapidly and the heat-carrying capacity of the loop to deteriorate, which in turn causes the reactor temperature rise. The introduced negative temperature reactivity reduces the reactor power, and eventually, the reactor outlet temperature rises to a maximum of 771.04°C, an increase of 23.52°C.

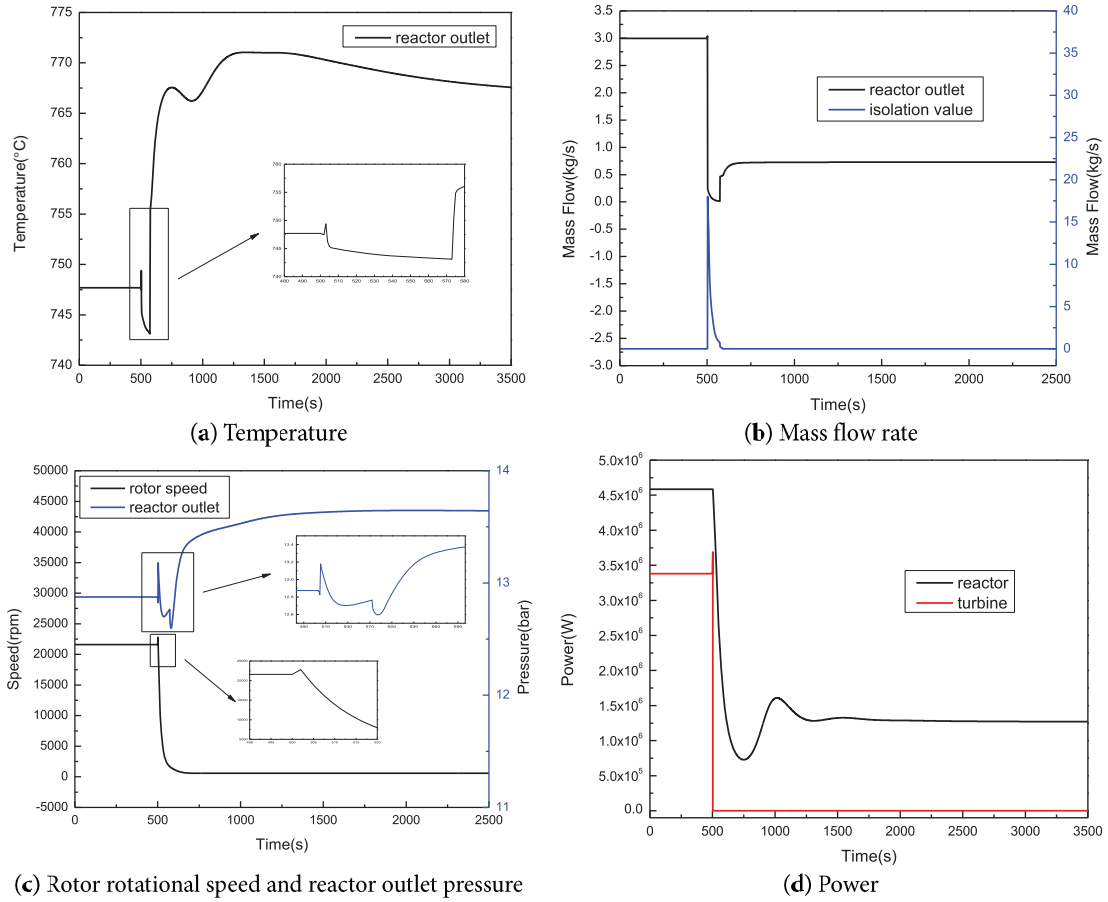


Figure 10: Main parameters variation diagram for load rejection operating condition: (**a**) Temperature; (**b**) Mass flow rate; (**c**) Rotor rotational speed and reactor outlet pressure; (**d**) Power.

Fig. 11 shows the change in turbine speed variations under different load rejection levels. It is evident that the turbine speed exhibits the most significant increase when the external load is completely lost.

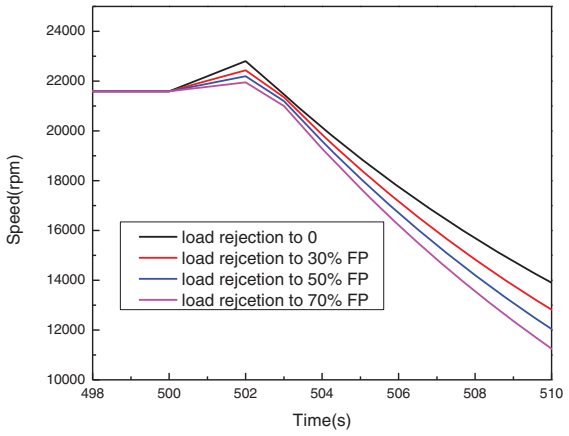


Figure 11: Main parameters variation diagram for load rejection operating condition.

5 Conclusion

This study has developed a complete dynamic analysis model for the MGCR using Modelica, which enables accurate simulation of the reactor's transient behavior. The validity of the model was verified through two levels of benchmarking, confirming the model's high accuracy and reliability, the steady-state verification against design values, and the transient verification against the MGT-3D code results.

In addition, transient analyses of reactivity insertion, loss-of-flow, and load rejection have been carried out, and the following conclusions are drawn:

The reactor exhibits an effective negative feedback mechanism. During the analyzed accident scenarios, this mechanism enables the reactor to quickly reach a new steady state or continuously reduce power, thereby ensuring the safety of the reactor without the need for external intervention.

During the reactivity insertion accident and the loss-of-flow accident, the negative feedback mechanism limits the reactor's maximum power. In the reactivity insertion accident, the maximum temperature rise at the reactor outlet is 33.89°C, and the net power increase is 0.22 MW. In the loss-of-flow accident, the reactor power does not increase significantly, and the maximum temperature rise at the reactor outlet is 23°C. Neither of these maximum temperature rises exceeds the reactor's safety limit.

For the load rejection event, the activation of the isolation valve effectively mitigates the turbine rotor overspeed. When the load is completely lost, the turbine rotor speed increases by a maximum of 5.6% relative to the rated rotor speed; meanwhile, the reactor power does not increase significantly, and the maximum temperature rise at the reactor outlet is 23.52°C, and all the key operating parameters remain within the allowable ranges.

Acknowledgement: The authors would like to express their sincere gratitude to China National Nuclear Corporation for the generous support and funding provided for this research.

Funding Statement: This research was funded by the centralized R&D project of China National Nuclear Corporation, grant number KY19105.

Author Contributions: Conceptualization, Yunlong Li; methodology, Yunlong Li and Yuer Zhao; software, Li Pan; validation, Yunlong Li, Yuer Zhao and Huimin Zhang; formal analysis, Huimin Zhang; investigation, Jun Wang; resources, Jun Wang; data curation, Yunlong Li; writing—original draft preparation, Yunlong Li; writing—review and editing, Yuer Zhao; funding acquisition, Jun Wang. All authors reviewed and approved the final version of the manuscript.

Availability of Data and Materials: Data available on request from the authors.

Ethics Approval: Not applicable.

Conflicts of Interest: The authors declare no conflicts of interest.

Nomenclature

A	Valve flow area
A_{He}	*He* flow path area
A_{max}	Maximum valve flow area
$A_{s,j}$	Block j heat transfer area
a_e	Pipe flow area
C_i	Group i delayed-neutron precursor concentration, where $i = 1, 2, \ldots, 6$
C_j	Block j specific heat
C_{min}	Minimum specific heat
$C_{p,\,He}$	*He* specific heat at constant pressure

C_q	Flow coefficient
D	Flow channel characteristic dimension
d_j	Block spacing
$dp_{He,j}$	*He* pressure drop
$l_{He,j}$	Volumetric channel length
h_{He}	Convective heat transfer coefficient of *He*
$h_{He,j}$	Block *j* thermal conductivity
h_{in}	Inlet enthalpy
$h_{in,nor}$	Rated inlet enthalpy
h_{out}	Outlet enthalpy
$h_{out,nor}$	Rated outlet enthalpy
Δh	Enthalpy different
K_t	Nonlinear coefficient
M_j	Block *j* flow rate
m_c	Cold side flow rate
m_h	Hot side flow rate
m_{He}	*He* flow rate
$m_{He,in}$	Inlet *He* flow rate
$m_{He,nor}$	Rated flow rate
$m_{He,out}$	Outlet *He* flow rate
Δm_{He}	Flow rate difference
n	Neutron density
n_I	*I* concentration
n_{Xe}	*Xe* concentration
p_{in}	Inlet pressure
$p_{in,nor}$	Rated inlet pressure
p_{out}	Outlet pressure
$p_{out,nor}$	Rated outlet pressure
Δp	Pressure difference
Δp_{max}	Maximum pressure difference
$\Delta p_{s,max}$	Maximum similar pressure difference
$\sum_f$	Fission cross section
Q_1	Energy released per fission
$Q_{f,j}$	Block *j* fission energy
$Q_{o,j}$	Block *j* energy inflow
$Q_{o,j-1}$, $Q_{o,j+1}$	Block *j* surrounding energy transfer
$Q_{s,j}$	Block *j* energy outflow
q_a	Actual heat transfer rate
q_c	Cold side energy change
q_h	Hot side energy change
q_{max}	Maximum heat transfer rate
T_{ave}	Average temperature
$T_{b,j}$	Block *j* ambient temperature
$T_{He,j}$	Block *j He* temperature
T_j	Block *j* average temperature
T_{ref}	Reference temperature
$t_{in,h}$	Hot side inlet temperature
$t_{in,t}$	Cold side inlet temperature
V_{He}	Volumetric flow rate

$V_{He,max}$	Maximum similar volumetric flow rate
$V_{He,min}$	Minimum volumetric flow rate
β	Total delayed neutron fraction
β_{i}	Group i delayed neutron fraction, where i = 1, 2, . . . , 6
γ_I	*I* fission yield
γ_{Xe}	*Xe* fission yield
η_e	Heat exchanger efficiency
η_h	Isentropic efficiency
$\eta_{\mathrm{h,nor}}$	Rated isentropic efficiency
η_m	Mechanical efficiency
$\kappa_{\mathrm{He,j}}$	*He* flow resistance coefficient
Λ	Prompt neutron life time
λ_{i}	Group i delayed neutron precursor decay constant, where i = 1, 2, . . . , 6
λ_I	*I* decay constant
λ_{Xe}	*Xe* decay constant
$\nu_{m,\ He}$	*He* flow velocity
ν_r	Rotor speed
$\nu_{r,nor}$	Rated rotor speed
ρ	Total reactivity
ρ_{CR}	Control rod reactivity
ρ_{in}	Inlet He density
$\rho_{in,nor}$	Rated inlet He density
ρ_{ini}	Initial reactivity
ρ_T	Temperature reactivity
ρ_{Xe}	*Xe* reactivity
τ	Torque
υ	Average number of neutrons per fission
ϕ	Neutron flux
χ_{Xe}	*He* thermal conductivity
α_T	Temperature feedback coefficient
ε	Pressure loss coefficient
μ	Conversion coefficient
ν_{flow}	Flow velocity
∂_{t}	Effective utilization coefficient
σ_a^{Xe}	Absorption cross section
Nu_{He}	Nusselt number
Re_{He}	Reynolds number
Pr_{He}	Prandtl number
u_d, u_q	Stator voltage *d*-*q* components
i_d, i_q	Stator current *d*-*q* components
Ψ_d, Ψ_q	Stator flux linkage *d*-*q* components
L_d, L_q	Stator winding *d*-*q* components
$\mathrm{R_s}$	Stator resistance
Ψ_r	Rotor permanent magnet flux linkage
T_e	Electromagnetic torque
T_L	Load torque
J	Moment of inertia
P	Rotor pole pairs
ω	Rotor angular velocity

References

1. Kang SW, Yim MS. Coupled system model analysis for a small modular reactor cogeneration (combined heat and power) application. Energy. 2023;262(7):125481. doi:10.1016/j.energy.2022.125481.
2. Ekinci F, Guzel MS, Acici K, Asuroglu T. The future of microreactors: technological advantages, economic challenges, and innovative licensing solutions with blockchain. Appl Sci. 2024;14(15):6673. doi:10.3390/app14156673.
3. Reid B, Sweetland K, Ward M. Advances in microreactor fabrication. Los Alamos, NM, USA: Los Alamos National Laboratory; 2023. Report No.: LA-UR-23-23350.
4. Mignacca B, Locatelli G. Economics and finance of small modular reactors: a systematic review and research agenda. Renew Sustain Energy Rev. 2020;118:109519. doi:10.1016/j.rser.2019.109519.
5. Rohbeck N, Xiao P. Evaluation of the mechanical performance of silicon carbide in TRISO fuel at high temperatures. Nucl Eng Des. 2016;306:52–8. doi:10.1016/j.nucengdes.2016.05.040.
6. Fritzson P, Engelson V. Modelica—a unified object-oriented language for system modeling and simulation. In: ECOOP'98—object-oriented programming. Berlin/Heidelberg, Germany: Springer; 1998. p. 67–90. doi:10.1007/bfb0054087.
7. Rabie MA, Elshahat AE, Hassan MH. Control oriented modeling of VVER-1200 using Modelica. Nucl Eng Des. 2024;420(5):112980. doi:10.1016/j.nucengdes.2024.112980.
8. Ding H, Lu DG, Sui DT, Zhang YL. Development of transient thermal-hydraulic analysis code for SCO_2-cooled reactor coupled with Brayton cycle and its application. Ann Nucl Energy. 2022;175:109255. doi:10.1016/j.anucene.2022.109255.
9. Qiu L, Liao S, Fan S, Sun P, Wei X. Dynamic modelling and control system design of micro-high-temperature gas-cooled reactor with helium Brayton cycle. Energy. 2023;278:128030. doi:10.1016/j.energy.2023.128030.
10. Wu H, Liu M, Liu S, Meng J, Chen S, Zheng R, et al. Development of system analysis code and its application in transient simulation of supercritical CO_2 Brayton cycle direct cooled reactors. Ann Nucl Energy. 2025;211:111031. doi:10.1016/j.anucene.2024.111031.
11. Li R, Wang X, Zhang L, Wang J. Development of tritium dynamic transport analysis tool for tritium breeding blanket system using Modelica. Fusion Eng Des. 2020;161:112023. doi:10.1016/j.fusengdes.2020.112023.
12. Ferrero S, Batet L, Linares JI, Arenas E, Cantizano A, Savoldi L. A Modelica dynamic model of a supercritical CO_2 energy conversion system for EU-DEMO. Fusion Eng Des. 2021;173:112826. doi:10.1016/j.fusengdes.2021.112826.
13. Liu T, Zhang Y, Zhao C, Huo H, Zhao Q, Chen W. Dynamic analysis of cold end accident conditions for a space gas-cooled reactor coupled with He-Xe Brayton cycle system. Int J Adv Nucl React Des Technol. 2025;7(3):294–307. doi:10.1016/j.jandt.2025.07.007.
14. Kastanya D. Evaluating the variations of point kinetics parameters in pressurized heavy water reactor analyses. Ann Nucl Energy. 2022;173(1):109130. doi:10.1016/j.anucene.2022.109130.
15. Wang K, Li Z, She D, Liang JG, Xu Q, Qiu Y, et al. RMC—a Monte Carlo code for reactor core analysis. Ann Nucl Energy. 2015;82:121–9. doi:10.1016/j.anucene.2014.08.048.
16. Kays WM, Crawford ME, Weigand B. Convective heat and mass transfer. Columbus, OH, USA: McGraw-Hill; 2011.
17. Incropera FP, Dewitt DP, Bergman TL, Lavine AS. Fundamentals of heat and mass transfer. Hoboken, NJ, USA: Wiley; 2007.
18. Daugherty RL, Ingersoll AC. Fluid mechanics. Columbus, OH, USA: McGraw-Hill; 1954.
19. Saravanamuttoo HIH, Rogers GFC, Cohen H. Gas turbine theory. Upper Saddle River, NJ, USA: FT Prentice Hall; 2001.
20. Cumpsty NA. Compressor aerodynamics. Hoboken, NJ, USA: Wiley; 2004.
21. Chung HY, Lo SL. Permanent magnet synchronous motor modeling and control. In: Proceedings of the 2014 International Conference on Fuzzy Theory and Its Applications (iFUZZY2014); 2014 Nov 26–28; Kaohsiung, Taiwan. p. 65–70.
22. Eriksson S. Permanent magnet synchronous machines. Energies. 2019;12(14):2830. doi:10.3390/en12142830.
23. Gou F, Liu Y, Chen FB, Dong YJ. Thermal behavior of the HTR-10 under combined PLOFC and ATWS condition initiated by unscrammed control rod withdrawal. Nucl Sci Tech. 2018;29(9):123. doi:10.1007/s41365-018-0472-3.

24. Baggemann J, Shi D, Kasselmann S, Kelm S, Allelein HJ, Hurtado A. Use of SANA experimental data for validation and verification of MGT-3D and a CFD porous media model for VHTR application. Nucl Eng Des. 2016;305:678–87. doi:10.1016/j.nucengdes.2016.05.030.
25. Tantillo F, Kasselmann S, Xhonneux A, Lambertz D, Trabadela A, Allelein HJ. HTR code package neutronics developments and benchmarks. Nucl Eng Des. 2020;362:110603. doi:10.1016/j.nucengdes.2020.110603.
26. Wright SA. Dynamic modeling and control of nuclear reactors coupled to closed-loop Brayton cycle systems using SIMULINKTM. AIP Conf Proc. 2005;746(1):991–1004. doi:10.1063/1.1867224.
27. Wu Y, Tang S, Zhu L, Lian Q, Zhang L, Ma Z, et al. Transient analysis of megawatt-level space gas-cooled reactor coupled with He-Xe Brayton cycle system. Appl Therm Eng. 2025;260:124962. doi:10.1016/j.applthermaleng.2024.124962.
28. Liu L, Zhu D, Liu M, Li D, Fu J, Guo H, et al. Transient analysis of the safety characteristics on a super carbon-dioxide cooled micro modular reactor. Nucl Eng Des. 2024;417:112866. doi:10.1016/j.nucengdes.2023.112866.